Unviersty of Anbar

Anbar Journal Of Engineering Science©

journal homepage: http:// http://www.uoanbar.edu.iq/Evaluate/

Numerical Investigation of Hydrothermal Performance of Pinned Plate-Fin Microchannel Heat Sink

Hamdi E. Ahmed [a*], Obaid T. Fadhil [a], Wesam M. Salah [a]

[a] Department of Mechanical Engineering, College of Engineering, University of Anbar Ramadi, Anbar, Iraq

PAPER INFO

Paper history:
Received 19 March 2018
Received in revised form 4 June 2018
Accepted 5 June 2018

Keywords:
Numerical simulation
Hydrothermal performance
Plate-fin heat sink
Oval pins

ABSTRACT

Enhancing the hydrothermal performance of plate-fin microchannels heat sink (*PFMCHS*) promises smaller size and lighter weight, and then improve the heat removal in consequently increase the speed of electronic devices.

In this numerical study, an innovative hydrothermal design of *PFMCHS* is suggested by inserting elliptic pins inside microchannels in different; aspect ratio (*AR*) of pin, pin number ratio (ψ) in order to optimize the hydrothermal design of this kind of heat sinks. The main objectives of this study are; investigating the effect of pins on the performance of *PFMCHS* by investigating the best geometry in the pinned-fin *MCHS* and which is higher, thermal or hydraulic performance of this kind of heat sinks and what is the optimal number of pins numerically and what about the pressure drop penalty in the proposed design, little, modest or high increase.

It is seen that the thermal resistance of the pinned fin *MCHS* is about 50% lower, and pressure drop of it is much higher than that of the (*PFMCHS*) under the condition of equal wind velocity. Maximum mechanical fan power reduction obtained is about 57% for the pinned fin *MCHS* with ψ = 1 and D_h = 1 ×10^{-3} m compared to the corresponding original channel heat sink. To show the overall performance of the two parameters; aspect ratio (*AR*), pin number ratio (ψ), the overall JF factor is estimated and the concrete findings shows that the best hydrothermal performance is obtained at the greater aspect ratio which is around overall *JF* = 1.2. In addition, the trend of overall *JF* is going down with the pin number ratio, starting from 1.2 to 1.15. And the concrete findings show that pinned fin *MCHS* provides thermal performance of 1.42 times greater than the smooth one under the corresponding conditions when one pin is used in each channel.

HIGH LIGHTS

- Hydrothermal design optimization of *PFMCHS* by inserting oval pins in the channels.
- The pin aspect ratio and numbers and orientations of the pins are optimized.
- One pin used in *PFMCHS* shows hydrothermal performance of 1.42 times greater than the original.
- Mechanical fan power reduction is 57% when the pins are sued getting the Nusselt number of the baseline.

- Pin aspect ratio of 0.45 shows overall *JF* factor of 1.2 with respect of the *PFMCHS*.

GRAPHICAL ABSTRACT

Top view of (Left) Vectors of velocity (m/s), and (right) Isotherm lines contours (k) for (a) *AR* = 0.138, (b) AR = 0.27, and (c) *AR* = 0.45 at *Re* = 1200, ψ = 1.

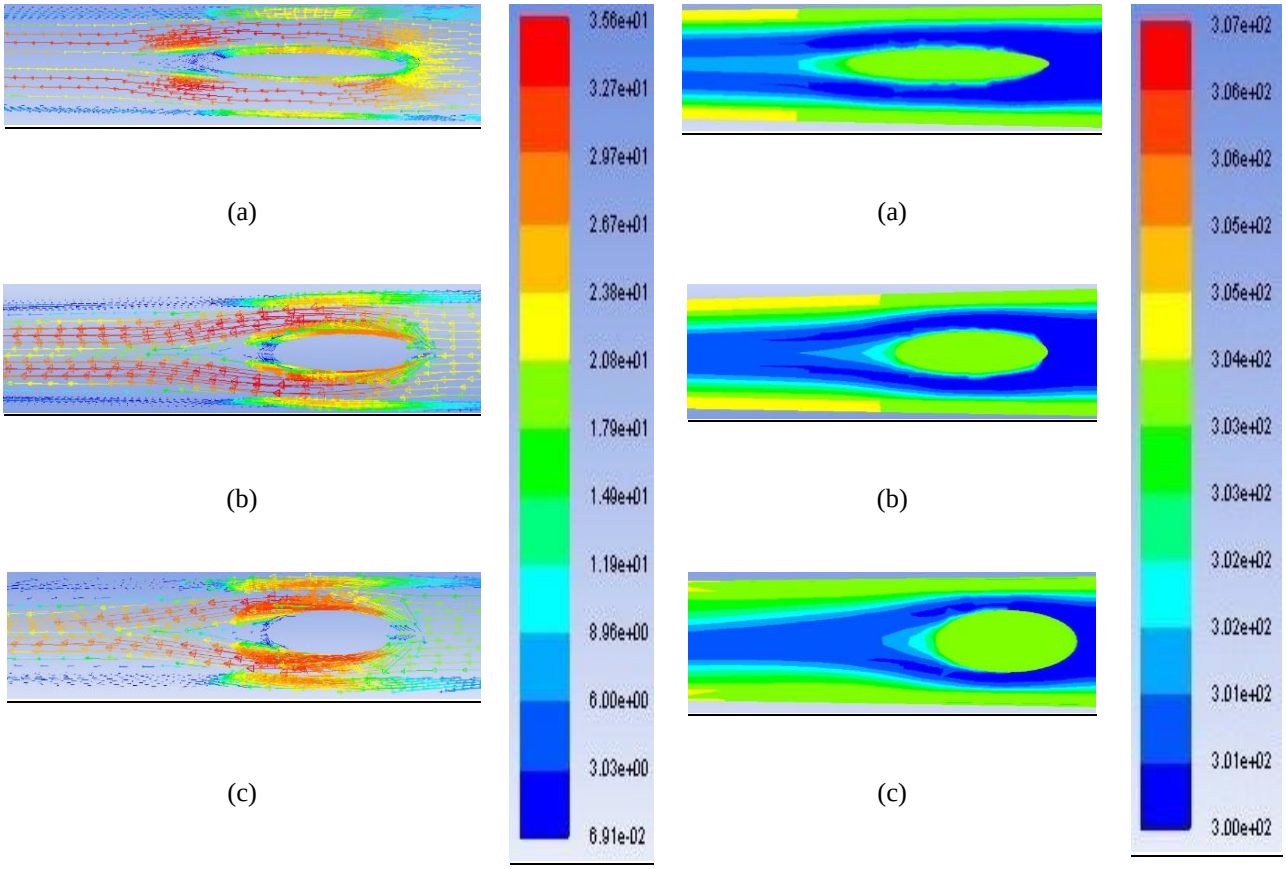

1. Introduction

Due to the progressing trend of integration, high performance and miniaturization of electronics industry, the requirement of higher performance of the electronic components becomes demanding. The density of the heat flow is increased with the decrement of the size of the components. However, high power densities result in increased junction temperatures, which adversely affect the reliability of electronic devices. Therefore, an effective cooling mechanism is essential for reliably operating electronic components. Many ideas pertaining to cooling methods have been proposed. Heat sinks are a kind of heat exchangers used for cooling the electronic devices due to the simplicity of fabrication, low cost, and reliability of heat dissipation [1]. The extended surfaces from the heat sinks are either flat-plate fins or pins fins shapes. In the last decades, intensive attentions were spent on miniaturizing the electronic devices because of the high sophisticated micro- and Nano-technology development. But the heat dissipation is still the major problem of enhancing the hydrothermal performance the heat sink. A comprehensive review is carried out on the methods used for optimizing the hydrothermal design of heat sinks. The purpose of this study is to summarize the investigational efforts spent for developing the hydrothermal performance of the heat sinks, therefore, oval pins have

been considered for studying here. Therefore, the methods of design and optimization of the heat removal devices is presented as follows: Based on plate fin heat sink (*PFHS*), ***Yu et al., [2]*** studied numerically and experimentally the effect of circular pins in *PFHS*. The simulation results showed that the thermal resistance of the pinned fin *HS* was about 30% lower than that of the original one under the same conditions. The profit factor define (*J=Q/P.P*) of the former was about 20% higher than that of the latter with the same pumping power. Another obvious advantage of pinned fin *HS* was that the user can change an existing unsuitable *PFHS* through planting columnar pins with different numbers or different geometry parameters into a required pinned fin *HS* by themselves to achieve better air-cooling results. ***Wang et al. [3]*** presented a ribbed *MCHS* with grooves for chips cooling. The micro-scale ribs and grooves were both fabricated on the heated wall of the *MCHS* to improve the laminar heat transfer rate. The results indicated that the Nusselt number of their proposed microchannels could be 1.11-1.55 times than that of smooth microchannel. At the same time, the utilizing of micro-scale ribs and grooves led to additional pressure drop penalty. They revealed that increasing the rib height showed the apparent friction factor ranged from 0.38 to 4.09 times above the smooth microchannel. ***Ahmed. [4]*** Has made a numerical study about innovative thermal design of *PFHS* through the insertion of ribs inside channels with different orientations, positions, sizes and numbers in order to obtain the optimal thermal design of this type of heat sinks. He investigated the effect of ribs on the thermal performance of *PFHS* while the number of fins was preserved constant, and ribs are inserted with a reduction in the number of fins simultaneously. The reduction was in terms of material saving by reducing the fins number, and reduction of the pumping power required while the fins number was kept constant to have a thermal performance as same as that of the original one. The specific findings inferred that ribbed *PFHS* provided a thermal performance of 1.55 times larger than *PFHS* under corresponding conditions. But the increment in the number of ribs reduced this improvement. The pumping power of ribbed PFHS reduced to 69.65% compared to the PFHS for the same thermal performance. Also, the hydrothermal performance of ribbed SFHS that have five channels with 15 ribs was 1.37 times better than nine smooth channels, and the substrate material reduced by 27.24%. ***Jonsson and Moshfegh [5]*** tested seven types of heat sinks including plate fin, strip fin, and pin fin heat sinks in a wind tunnel. Both in-line and staggered arrays had been studied having square and circular cross-sections for the pins in macro-scale, while the number of the duct Reynolds ranged from 2000 to 16,500. The pressure drop for the pin fin heat sinks was larger when compared to the strip fin heat sinks at high Reynolds values, while the variance in the thermal resistance remained marginal. Consequently, the use of pin fin heat sinks at high Reynolds numbers didn't bring any benefits. A numerical study was present by ***Hong and Cheng [6]***, it was about laminar forced convection of water in offset strip-fin *MCHS* for microelectronic devices cooling. It was found that there was an optimal strip-fin size to minimize the pumping power, and this optimal size depended on the input heat flux and the maximum wall temperature. Experimental investigation was carried out by ***Liu et al., [7]*** for studying the behavior of heat transfer and pressure drop for liquid flow in rectangular microchannels with several rows of *VGs*. Laminar and turbulent flow regime with hydraulic diameter of the micro-channel of 187.5 μm and three rectangular block *LVGs* were implemented in stream-wise way of the rectangular microchannels with changed numbers of *VG* pairs and angles of attack. They originate that the range of Reynolds numbers (600–730) were at a much lesser value by adding *LVGs* than the that deprived of *VG* (*Re* ≈ 2300); Heat transfer presentation was enhanced nearly (9–21% higher for those with laminar flow and 39–90% for those with turbulent flow), while encountering larger pressure drop (34–83% for laminar flow and 61–169% for turbulent flow). ***Kim et al., [8]*** studied mixing based on mass diffusion and advective flow at low Reynolds number because of its importance on the design of microscale vortex generators. Four vortex generators geometries simultaneously; vortex generators angle, vortex generators height, vortex generators width, and vortex generators spacing were considered. The optimized microchannel was found at a micromixer configuration where *VG* angle, *VG* height ratio, *VG* width ratio and space of *VG* ratio to *VG* height were 35.6°, 0.7, 0.127, and 1.10, respectively. The channel length to obtain the mixing uniformity over 95% was 1344 μm. ***Yi Li et al., [9]*** reported both experiments and numerical simulations investigating the thermal-fluid physiognomies of a smooth-fin *HS* with a couple of *VG* connected in a cross-flow channel before the leading edge of the HS. The effect of geometric and orientation parameters of *VG* were examined. It was found from the results that in small distance between trailing edges of the *VG* the thermal performance was bad due to the difficulty in the airflow into *HS*. The optimum performance was reached through making the space between the trailing edge of each

VG and the front finale of the *HS* zero and the distance between the *VG* trailing edges equal the length of the *HS*. In order to optimize the pressure difference and thermal resistance, an attack angle of the *VG* of 30 degrees was preferred. Although the heat transfer increased with the height of the *VG*, the pressure difference also increased. The heat transfer enhancement of the *HS* by using *VG* was greater, and the increase of the pressure difference was lower, at lower Reynolds numbers. ***Ebrahimi et al., [10]*** conducted a numerical investigation for laminar water flow and heat transfer performance of in rectangular microchannels provided with longitudinal *VG*. Their results showed that for Reynolds number reached from 100 to 1100, there was a 2–25% rise in the Nusselt number for microchannels with *LVGs*, while the friction factor raised by 4–30%. Except one at *Re* = 100, the total presentation of the all shapes of microchannels with *LVGs* was advanced than ones without *LVGs*. ***Zhuo et al., [11]*** presented three-dimensional numerical simulations of laminar flow and heat transfer of water in silicon microchannels with trapezoidal and triangular cross-sections. Their solutions showed that when *Re* number was lesser than 100, the combined effect between velocity and temperature gradient was much improved than the case of *Re* > 100. There was an abrupt change in the intersection angle between velocity and temperature gradient around *Re* = 100. For the two microchannels, the heat transfer strength of the trapezoidal microchannel was much improved than that of the triangular one, which shows the significant impact of the geometric condition in microchannel system. In addition, for the two microchannels, the rise of *Re* number caused an increment in the Nusselt number in the fully developed zone, seemingly changed from that of conventional duct, where the Nusselt number of the fully developed laminar heat transfer was unchanging. ***Xia et al. [12], and [13]*** investigated different geometric parameters of *MCHS* with triangular reentrant cavities on water flow and heat transfer characteristics numerically. In order to find the optimum geometric parameters, four variables, representing the distance and geometry of the triangular reentrant cavity, were designed. It was found that the vortices in the triangular reentrant cavities led to chaotic advection and could greatly enhance the convective fluid mixing. And he carried out an investigation of fluid flow and heat transfer characteristics in a *MCHS* with offset fan-shaped reentrant cavities in sidewall. Steady and laminar flow regime were considered in their study, they pointed out that the proposed plan enhanced heat transfer presentation associated with an acceptable pressure drop attributed to the communication of the improved heat transfer surface area, the redeveloping of the hydraulic and thermal boundary layers, the jet and throttling upshots and the slipping over the reentrant cavities. ***Wang a et al. [14]*** proposed different cannelure fin structure applicable to compact air-cooled heat sink under cross-flow condition. Test results indicated that approximately 25% of heat transfer performance increment can be achieved by the proposed full cannelure fin along with the dimple/cavity structure, and the friction abridged of about 20%. Furthermore, converse to those interrupted fin or triangular *VG*, it was found that a significant augmentation was offered by the proposed fin structure in fully developed region. The possible mechanism for appreciable increase of heat transfer without suffering the pressure drop penalty was attributed to the local suction/blowing flow and the near wall vertical motion caused by the cannelure structure. ***Ahmed and Ahmed [15]*** have conducted a three-dimensional numerical simulation for investigating the changed caused by geometric parameters in the characteristics of laminar water flow and forced convection heat transfer in grooved *MCHS*. Their examination included the orientation, tip length, depth and pitch of the cavities for improving the hydrothermal performance of an aluminum heat sink plan. The shape of cavity can be improved by these geometric parameters, from triangular to trapezoidal and then to rectangular shape. The results presented that the trapezoidal groove with groove tip length ratio of 0.5, groove depth ratio 0.4, groove pitch ratio of 3.334, grooves orientation ratio of 0.00 and *Re* = 100 was the optimum thermal plan with Nusselt number improvement of 51.59% and friction factor improvement of 2.35%. In the paper of ***Mohammed et al., [16], and [17]*** Laminar heat transfer and water flow characteristics in wavy *MCHS* with rectangular cross-section with various wavy amplitudes ranges, was numerically investigated. It was displayed that heat transfer performance of the wavy microchannels was improved than the straight microchannels. The pressure drop penalty of the wavy microchannels was reduced than the heat transfer improvement. The friction factor was increased proportionally as the amplitude of wavy microchannels increased. And he tested numerically the heat transfer and laminar water flow behavior in *MCHS* having zigzag, curvy, and step microchannels shapes. They highlighted that for the similar cross-section of a *MCHS*, the temperature and the heat transfer coefficient of the zigzag *MCHS* was the smallest and highest, respectively, among various channel shapes. The pressure drop penalty for all channel shapes was advanced

than the conventional straight *MCHS*. The zigzag *MCHS* had the highest rate of pressure drop, and friction factor monitored by the curvy and step *MCHS*, respectively. ***Rahman [18]*** presented experimental measurements for pressure drop and heat transfer coefficient of water in *MCHS*. Two different channel patterns were designed to see the effects of flow branching, channel length, and fluid velocity. The parallel pattern (*I-channel*) distributed the fluid through several parallel passages between the inlet and the outlet headers located at two ends of the wafer. The series pattern (*U-channel*) carried the fluid through a longer winding channel between the inlet and the outlet headers. The larger heat transfer was caused by the breakage of velocity boundary layer by surface roughness associated with etched channel structure. The transition from laminar to turbulent flow was somewhat gradual because of small channel dimension. The research of ***Shaalan et al., [19]*** goal was to study the impact of the use of heat shield on the performance of a parallel *PFHS* experimentally and numerically in turbulent flow regime. It was found that the thermal resistance could be reduced through attaching a shield to the heat sink, especially at low Reynolds number. And a complicated variation in flow field around the *HS* and its thermal performance can be caused by changing the angle of shield inclination. It was found that the inclination angle that yielded minimum thermal resistance varies with *HS* height. For shortest fin height used (H =15 mm), this resistance was minimum with range ($30° < \theta < 90°$), while for higher *HS* heights, the optimum heat shield angle ranged between 120° and 135°. The surface temperature of the base of the *HS* was analyzed by ***Li Et al. [20]*** to determine the changes in the thermal resistance caused by Reynolds number, shield, and height and fin width. The bypass flow effect was decreased by due to the introduction of a shield which also forced more coolant fluid to enter the channel from fin to improve the heat transfer. The thermal resistance of the HS is reduced by the Reynolds number, but that decrease tended to be minimized with increase of Reynolds number. When the Reynolds number attained a certain value the improvement of heat transfer by the heat sink became limited. For a given fin width, the thermal performance of the *HS* with the highest fins was superior. For a given fin height, the optimal fin width in terms of thermal performance increased with increasing Reynolds number. As the fins became wider, the flow passages in the *HS* constricted the entrance of coolant air; as the fins became narrower, the area of heat transfer of the *HS* decreased. Both conditions caused a decrease in the heat transfer of the *HS*. Most recently, the review paper of ***Hamdi et al. [21]*** is summarizing the investigational techniques which were used for improving the hydrothermal performance of *HS*. In addition ,they reported the research gaps that still under research and need more focus by investigator, The varying of the fin number, fin geometry, channel shape, channel aspect ratio, grooved channel, and ribs and turbulators in between channels have an attractive effect for getting the optimal thermal design of the heat sinks. Baffles, vortex generators, and ribs showed better hydrothermal performance more than smooth heat sinks. The miniaturization of the heat sinks showed excellent results in both hydraulic and thermal performance. There was no paper refers to examine the effect of oval pins in plate-fin microchannel *HS*. ***Wahid et al. [22]*** studied numerically simulation the heat transfer characteristics and pressure drop of Nanofluids in compact heat exchanger with different tube shapes and an in-line arrangement of tubes under steady-state laminar fluid flow. The results revealed that the enhancement of heat transfer. In addition, it was accompanied by acceptable pressure drop values in comparison with the circle and elliptic tube shapes in compact heat exchangers, it can be clearly seen that the elliptic tube bank heat exchangers provides lower frictional losses compared to flat-tube as well as circular tube. The overhead literature review and due to the finest knowledge of the authors show that in the past the optimization of thermal design of *MCHS* using plate-fin microchannel heat sink with oval pins has not been investigated. Also, it is very clear that *MCHS* was extensively studied but the reported data is limited in the literature that involves non-circular pins. In this numerical research, an innovative thermal design of (*PFMCHS*) is suggested by inserting pins inside channels in dissimilar sizes, positions, and numbers of the pins in order to get an ideal thermal design of this kind of heat sinks. The central objectives of this study are; investigating the effect of pins on *MCHS*. The present study is proposed to develop the work of ***Yu et al., [2], Jonsson and Moshfegh [5]*** by using new oval pins (elliptical pins) with air as working fluid which has not been studied yet. This gap motivated the present study to examine this area of research numerically in three dimensions. The results of parameters such as Nusselt number, friction factor, *JF* factor, pressure drop and mechanical fan power and streamlines and isotherm lines contours will be depicted, compared with those of smooth-fin microchannels and thoroughly explained to illustrate the effect of various parameters on the *MCHS* performance.

2. Mathematical Formulation

2.1 Physical statement and assumption

The schematic diagram of the physical problem considered in this research is shown in Figure.1. The area of the bottom of the substrate is ($50\times10.1\times 10^{-6}$) m^2 (i.e., width (W) × length (L)). The height and the width of the fin are ($H_f = 1.125\times 10^{-3}$m and $W_f = 0.2 \times 10^{-3}$ m), respectively. The height of the base of the substrate is ($H_b = 0.5\times 10^{-3}$ m). The number of the fins (N_f) of the *MCHS* is (10). The width of the channel is = 0.9×10^{-3}m. Oval pins (elliptical pins) are suggested and considered in each channel, attached on the bottom of the flow channel and has same circumferential area of the pin (exposed to the fluid) and the circumferential area of the pin is ($A = 0.35\times 10^{-6}$ m^2) (where, $A = \pi\times r\times R$). The small and large diameter of the oval pin is (d = 0.45, 0.35, 0.25×10^{-3}m and D = 1.0, 1.285, 1.8×10^{-3}m), respectively, is varied along the tests, one height is considered for the oval pins. The value of the pitch distance (S) between the beginning of the channel and the pin center is (5×10^{-3}m). The range of the varied parameters are shown in Table 1. The parameters varied along this study are; aspect ratio, number of pins, mechanical fan power with wide range of Reynolds number. The first optimization parameter is the aspect ratio which is defined as (ratio of small to large diameter of elliptical pin) ($AR = d/D$) while *ARs* are (0.138, 0.27, and 0.45), respectively. The second optimization parameter is the pin number ratio which is mathematically defined as ($\psi = N_p/N_c$) and has the values of (0, 1, 2 and 3). Last parameter investigated in this study is the thermal resistance reduction and pressure drop and mechanical fan power reduction between the channels. The heat flux supplied to the bottom of the substrate block is considered (q =1500 W/m^2) in which the temperature of the base of the substrate doesn't exceed 70º C in the case of smooth channels and at lowest value of Reynolds number [2]. The geometric parameters of the plate-fin *MCHS*, pinned fin *MCHS*, and the computational domain and the pin dimensions are illustrated in Figure.1. (a)– (e). Using air as a working fluid, the following assumptions are considered for heat transfer and fluid flow characteristics in the pinned fin *MCHS*:

- Three-dimensional fluid flow, incompressible and steady-state.
- Laminar forced convection heat transfer and constant wall heat flux.
- Negligible radiation heat transfer.

At the microchannel sections, the inlet air temperature is taken as ($T = T_m = 300\ K$) and the inlet air velocity is calculated based on the required Reynolds number. In calculating the velocity, the air is assumed to be uniform distributed into all *MCHS*. The transverse velocities at the inlet are assumed zero. On the aluminum substrate, the velocities are zero, and it is assumed the top plate of the *MCHS* to be an adiabatic surface. The initial fluid velocity and temperature at the inlet is taken as the mean velocity u_m and mean temperature T_m. Therefore, the initial boundary conditions can be written as follows

$$u = u_m,\ \ v = w = 0$$

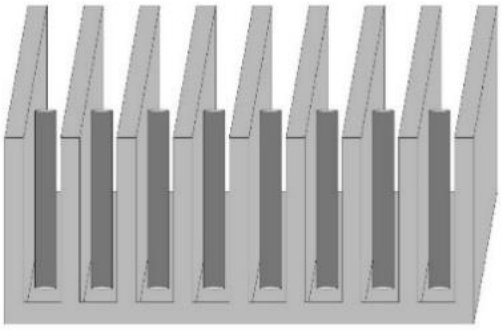

(a)

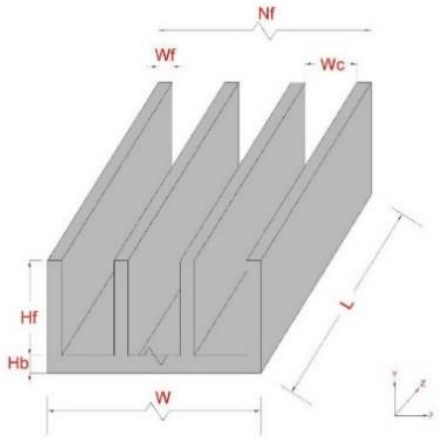

(b)

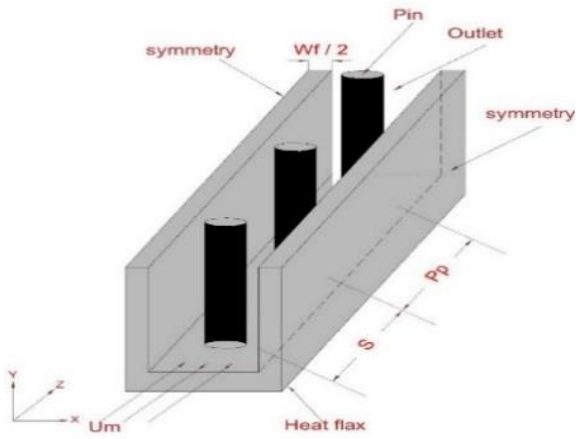

(c)

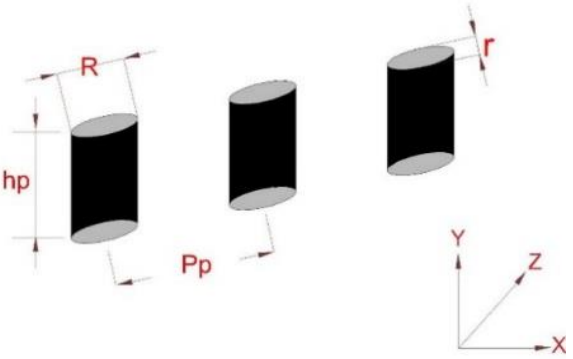

(d)

Figure.1. Schematic diagram of (a) pinned fin *MCHS*, (b) geometric parameters of *PFMCHS*, (c) computational domain, and, (d) geometric parameters of pin. The scheme is not drawn to scale.

Table 1. Variables of geometric parameters considered for optimization.

Symbol	*definition*	*Equation/note*	*Domain*
Wc	width of the channel	-	0.9×10^{-3}m
d	small diameter of pin	-	0.45, 0.35, 0.25$\times 10^{-3}$m
D	large diameter of pin	-	1, 1.285, 1.8$\times 10^{-3}$m
H_p	pin heights	-	1.125$\times 10^{-3}$m
N_f	number of the fins	-	10
P_p	pin pitch	-	10×10^{-3}m
N_P	number of pins	*in each channel*	0, 1, 2, 3
D_h	hydraulic diameter	-	1×10^{-3}m
AR	Aspect ratio	$AR = d/D$	0.45, 0.27, 0.138
ψ	pin number ratio	N_P/N_c	0, 1, 2, 3
Re	Reynolds number	$\rho\, U\, D_h/\,\mu$	100, 250, 500, 800, 1200

2.2 Governing equations

The continuity, momentum, and energy governing equations in non-dimensional form for steady, laminar and incompressible flow, in Cartesian coordinates are Continuity equation [15]:

$$\frac{\partial U}{\partial X}+\frac{\partial V}{\partial Y}+\frac{\partial W}{\partial Z}=0 \qquad (1)$$

X − Momentum equation:

$$U\frac{\partial U}{\partial X}+V\frac{\partial U}{\partial Y}+W\frac{\partial U}{\partial Z}=-\frac{1}{\rho}\frac{\partial P}{\partial X}+\mu\left(\frac{\partial^2 U}{\partial X^2}+\frac{\partial^2 U}{\partial Y^2}+\frac{\partial^2 U}{\partial Z^2}\right) \qquad (2)$$

Y − Momentum equation:

$$U\frac{\partial V}{\partial X}+V\frac{\partial V}{\partial Y}+W\frac{\partial V}{\partial Z}=-\frac{1}{\rho}\frac{\partial P}{\partial Y}+\mu\left(\frac{\partial^2 V}{\partial X^2}+\frac{\partial^2 V}{\partial Y^2}+\frac{\partial^2 V}{\partial Z^2}\right) \qquad (3)$$

z − Momentum equation:

$$U\frac{\partial W}{\partial X}+V\frac{\partial W}{\partial Y}+W\frac{\partial W}{\partial Z}=-\frac{1}{\rho}\frac{\partial P}{\partial Z}+\mu\left(\frac{\partial^2 W}{\partial X^2}+\frac{\partial^2 W}{\partial Y^2}+\frac{\partial^2 W}{\partial Z^2}\right) \qquad (4)$$

Energy equation:

$$U\frac{\partial \theta}{\partial X}+V\frac{\partial \theta}{\partial Y}+W\frac{\partial \theta}{\partial Z}=\vartheta\left(\frac{\partial^2 \theta}{\partial X^2}+\frac{\partial^2 \theta}{\partial Y^2}+\frac{\partial^2 \theta}{\partial Z^2}\right) \qquad (5)$$

Where ϑ the kinematic viscosity is defined as $k/(\rho c_p)$. The non-dimension parameters are defined as:

$$X=\frac{x}{Dh},\ Y=\frac{y}{Dh},\ Z=\frac{Z}{Dh},\ U=\frac{u}{um},\ V=\frac{v}{um},\ W=\frac{w}{um} \qquad (6)$$

Where θ stands to the dependent parameters u,v and w and T. In the above equation, the u,v and w are the velocity components in x, y and z directions, respectively, and P is the pressure and T is the temperature.

2.3 Boundary Condition: The boundary conditions of the above set of governing equations are as follows:As ($T = T_m = 300\ K$) and (q =1500 W/m^2).

i- At the inlet of channel:

$$u = u_{in},\ v = w = 0,\ T = T_{in} = 300K$$

at

$$W_f/2 \le x \le W_c + W_f/2;\ H_b \le y \le H_b + H_f;\ z = 0$$

ii- At the exit of channel:

$$\frac{\partial u}{\partial z}=\frac{\partial v}{\partial z}=\frac{\partial w}{\partial z}=\frac{\partial T_f}{\partial z}=0,\ p = p_{out} = 1atm$$

at

$$W_f/2 \le x \le W_c + W_f/2;\ H_b \le y \le H_b + H_f;\ z = L$$

iii- At the upper wall:

$$u = \nu = w = 0;\ -k_w \frac{\partial T_w}{\partial Y} = 0$$

at

$0 \le x \le W_c + W_f;\ y = H_b + H_f;\ 0 \le z \le L$

iiii- At the internal sidewalls and lower wall of channel:

$$u = \nu = w = 0;\ -k_w \frac{\partial T_w}{\partial X} = q$$

at

$x = W_f/2;\ H_b \le y \le H_b + H_f;\ 0 \le z \le L$

OR $$u = \nu = w = 0;\ -k_w \frac{\partial T_w}{\partial X} = q$$

at

$x = W_c + (W_f/2);\ H_b \le y \le H_b + H_f;\ 0 \le z \le L$

v- At the lower heated wall of substrate HS

$$u = \nu = w = 0;\ -k_w \frac{\partial T_w}{\partial Y} = q$$

at

$W_f/2 \le x \le W_c + (W_f/2);\ y = H_b;\ 0 \le z \le L$

vi- At the Sidewalls of substrate HS (symmetry)

$$u = \nu = w = 0;\ -k_w \frac{\partial T_w}{\partial Y} = q$$

at

$0 \le x \le W_c + W_f;\ y = 0;\ 0 \le z \le L$

vii- Front and back wall of substrate HS

$$\frac{\partial u}{\partial x} = \frac{\partial_w}{\partial X} = \frac{\partial T_f}{\partial X} = \frac{\partial T_w}{\partial X} = 0,\ \nu = 0$$

at

$x = 0,\ 0 \le y \le H_b + H_f;\ 0 \le z \le L$

$x = W_c + W_f;\ 0 \le y \le H_b + H_f;\ 0 \le z \le L$

OR $$-k_w \frac{\partial T_w}{\partial z} = 0$$

at

$0 \le x \le W_c + W_f;\ 0 \le y \le H_b + H_f;\ z = 0$

$0 \le x \le W_c + W_f;\ 0 \le y \le H_b + H_f;\ z = L$

2.4 Grid Independent Test

The grid independent test is examined in order to obtain an appropriate grid system. Eight different sizes of grid are tested to check the effect of the grid density on the computational results. The mesh generated for the present analysis consists of 556,021 elements and 621,124 nodes. And the relative error between the fourth and fifth grid is (*Nu* error 0.071%, *f* error of 0.42%). The grid independence test is carried out by varying elements from 237,207 to 1075,052 in eight steps for $Re = 1200$, $\psi = 1$ and $AR = 0.27$. The increase in mesh elements after 621,124 has less than 1% variation in Nusselt number and friction factor and gives a very slight deviation and shorter time for iteration compared with other finer grids is adopted in this study as shown in. So the mesh with 621,124 elements is taken as criterion for grid independence and is used for carrying out numerical analysis for the cases investigated in this study. It is worthy to be mentioned that the finest grid (Eight grid) is tested to make sure that there is no change in (Nu_{avr} *and f)*. As shown in ***Figure.2. (a)-(b)***, which show the results of the grid independence test and relative error *of* Nu_{avr}*% and f %*, the grid number (621,124) is employed.

The relative error is;

$$E_M\ \% = \left|\frac{M_{MAX} - M_{MIN}}{M_{MAX}}\right| \times 100 \qquad (7)$$

Where *(M)* represents any parameter. ***Figure.3. (a)-(b)*** shows the structured mesh used in the *CFD* simulation.

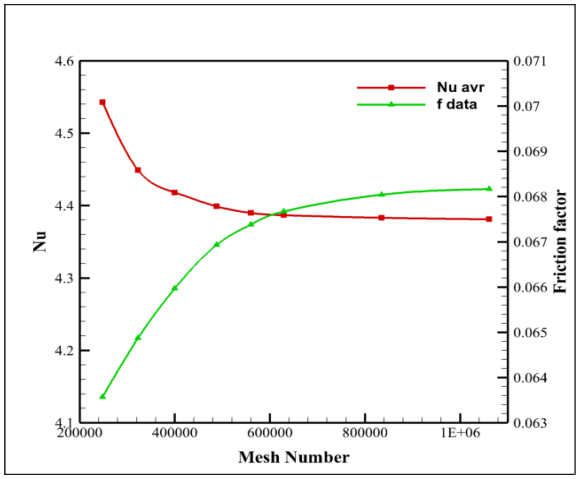

(a)

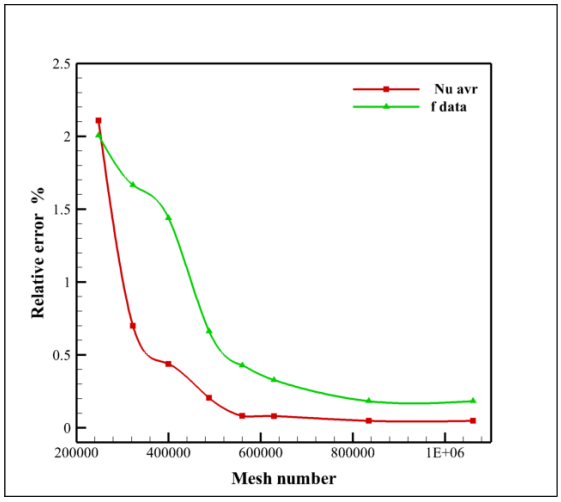

(b)

Figure.2. the results of the grid independent test (a) Nu_{avr} *and f data (b)* relative error *of* Nu_{avr}*% and f %.*

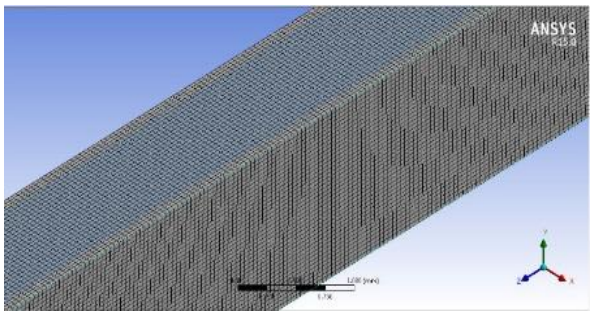

(a)

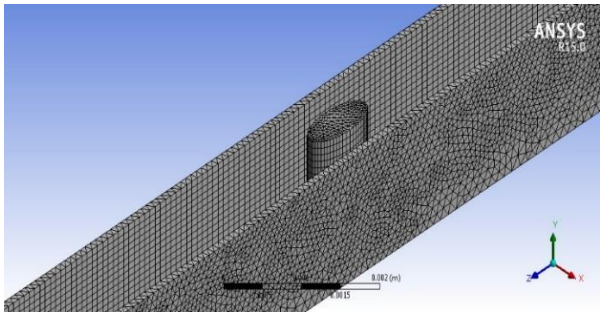

(b)

Figure.3. *(a) Meshing of the domain, and (b) meshing of pin.*

3. Numerical Procedure

3.1 Solution Method

The finite volume method (*FVM*) is used to solve the governing equations with corresponding boundary conditions by using the commercial computational fluid dynamics (*CFD*) package (Fluent v.15.0). The convective term of 2nd order method implementing the SIMPLE algorithm is employed for the pressure and velocity coupling. The diffusion term in the momentum and energy equations is approximated by 2nd order upwind. A uniform structured mesh is generated for the whole domain except the zone of pin in which non-uniform, unstructured, finer and high concentration mesh is applied. The iteration of simulations is continued until the sum of normalized residual of all components became negligible (less than 10^{-5}) and velocity components does not alter from each other iteration. The residual sum for each of the conserved variables is computed and stored at the end of each iteration, thus recording the convergence history. Moreover, the convergence criterion demanded that the maximum relative mass residual based on the inlet mass became smaller than 10^{-10}.

3.2 Numerical Calculation

The local convection heat transfer coefficient and local Nusselt number respectively are estimated as follows [4],

$$h_z=\frac{Q}{A_h\times(Twz-Taz)} \quad (W/m^2K) \qquad (8)$$

$$Nu_Z=\frac{h_z\times D_h}{K} \qquad (9)$$

Where T_w and T_a, the average heated wall temperature and the average air bulk temperature, respectively.

The A_h is estimated by

$$A_h=(2H_f+W_C)\times L \quad (m^2) \qquad (10)$$

Where A_h the convection heat transfer area.

Reynolds number is calculated from the following formula

$$Re=\frac{\rho\times U\times D_h}{\mu} \qquad (11)$$

Where D_h is the hydraulic diameter of the channel which is calculated as follows

$$D_h=4\frac{Ac}{P}=2\frac{W_C\times H_f}{(H_f+W_c)} \quad (m) \qquad (12)$$

Where A_c represents the cross-sectional area of the channel flow and P represents the wetted perimeter

of the channel. The friction factor in the channel is calculated by

$$f = \frac{2D_h \times \Delta P}{LC \times \rho \times (U_m)2} \quad (13)$$

The hydrothermal performance evaluation factor (*JF*) is defined by Webb and Eckert (1972), [15], [23], and [24] and is given as,

$$JF = \frac{(Nu^*/Nu^o)}{(f^*/f^o)\hat{}(1/3)} \quad (14)$$

The mechanical fan power (*M. F.P*) required to propel a volumetric flow rate ($\dot{V}$) at a pressure drop Δp is estimated from

$$M.\ F.P = \dot{V} \times \Delta p = u_m \times A_C \times \Delta p \quad \text{(W)} \quad (15)$$

Where the cross-sectional area for one channel is calculated by

$$A_C = H_f \times W_C \quad (m^2) \quad (16)$$

In evaluating the thermal performance of the heat sink, the thermal resistance is defined as:

$$R_{th} = \frac{\Delta T}{Q} = \frac{T_b - T_a}{Q} \quad \text{(K/W)} \quad (17)$$

Where ΔT is temperature difference between the highest temperature on the fin base and the ambient air temperature, T_b is the mean base plate temperature and T_a is the temperature of the cooling air. And Q is heat dissipation power applied on the fin base.

3.3 Validation of the Plate- Fin MCHS

In order to validate the model output, the axial variation of the longitudinal *Nu* numbers of the smooth fin MCHS has been firstly compared with the numerical data of ***Zhuo et al., [11]*** for a numerical study of laminar convective heat transfer in microchannel with (trapezoidal and triangular) cross-sections are performed as shown in ***Figure 4. (a) and (b)***, respectively. Both comparisons of the longitudinal Nusselt number of trapezoidal and triangular microchannel show excellent agreement with the literature are within ± 2%.

The variation of the thermal resistance and pressure drop of the pinned-fin *MCHS* has been secondly compared with the experimental data of ***Jonsson and Moshfegh [5]*** and the numerical results of ***Yu et al., [2]*** for laminar convective heat transfer in in-line circular pin fin *MCHS*, as shown in ***figure 5. (a) and (b)*** respectively. As can be seen in the figure, agreement accepted has been obtained of experimental data and numerical results and the present simulation data for both thermal resistances and pressure drops are within ± 5%.

The third compared to validate the computations, smooth plate-fin *MCHS* are validated with the experimental measurements of ***Sohel et al., [25].*** They performed number of experiments on smooth mini-channel heat sink. A comparison is held between the current numerical results and experimental measurements as shown in ***Figure 6 (a) and (b)***. The comparisons are in term the heat sink base temperature and heat transfer coefficient of pure water. This Figure illustrates that the present numerical output and the experimental results are close to each other are within ± 4%. For that reason, with valid numerical modeling, the computations of the heat sink with a pin will be conducted.

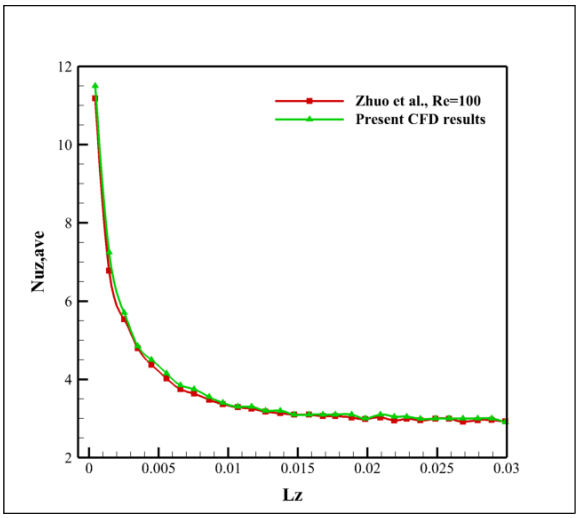

(a)

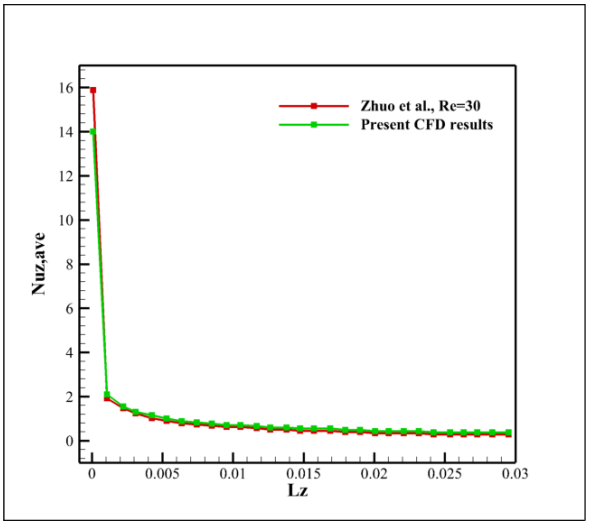

(b)

Figure.4. (a) Longitudinal *Nu* numbers variation for *Re numbers* = 100 of trapezoidal microchannel, (b) Longitudinal *Nu* numbers

variation for *Re numbers* = 30 of triangular microchannel ***Zhuo et al., [11].***

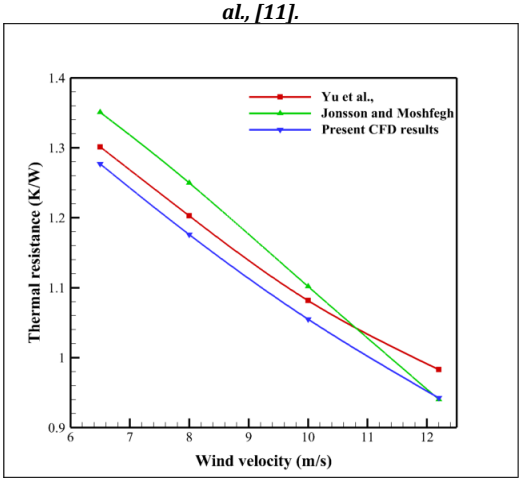

(a)

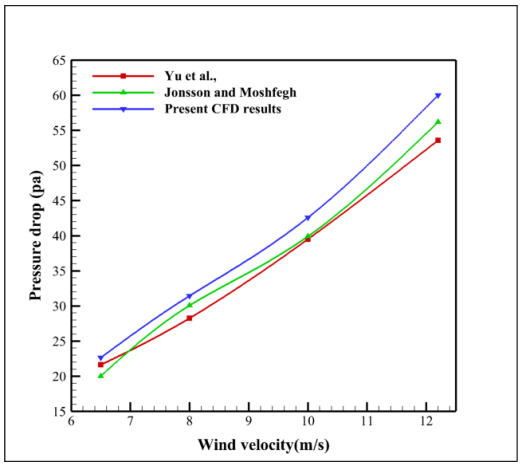

(b)

Figure.5.Validation of present *CFD* outcomes with ***Jonsson and Moshfegh [5]***, and ***Yu et al., [2]*** for (a) thermal resistances; (b) pressure drops.

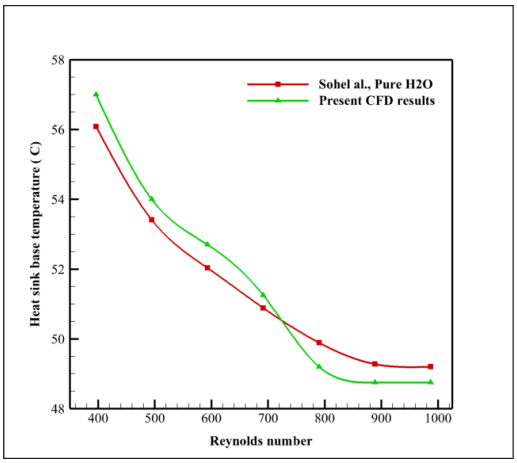

(a)

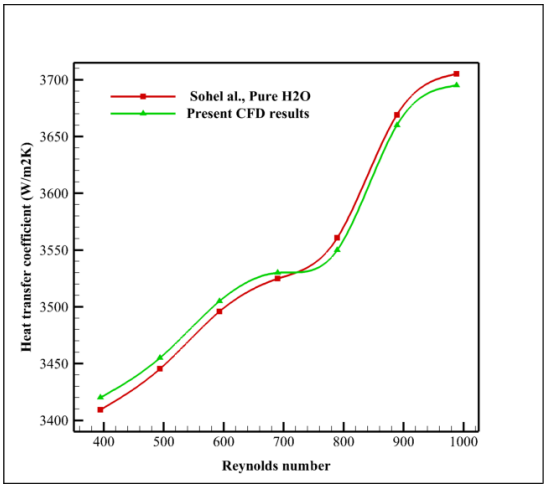

(b)

5. Result and dissection

As explained earlier, the main objective of the current study is to optimize the hydrothermal design of plate-fin microchannel heat sink by using new design of microchannel heat sink by inserting elliptic pins. This optimization is planned to be achieved by considering the main goal; is the enhancing the hydrothermal design of the heat sink. For this goal, several parameters are considered here; the aspect ratio (d/D), the number of pins, mechanical fan power reduction. In this work, three-dimensional numerical simulation for laminar airflow and forced convection heat transfer in plate-fin microchannel heat sink under a thermal condition of constant wall heat flux at the bottom of the substrate is considered. Generally, under $q = 1500\ W/m^2$ and for a range of Reynolds numbers (100−1200). The above different design variables of pins are considered in order to optimize the heat sink design. The results of heat transfer and pressure drop are represented in term of Nusselt number, friction factor, *JF* factor, vectors plots of velocity and temperature streamline contours are depicted and analyzed. It is worth to be mentioned that the contours of velocity and temperature are estimated at h_p = 0.3125mm to let the shortest pin to be seen in the contours, a recirculation and fluctuation in the fluid flow can be seen at and after the location of the pins occurs in this level making better fluid mixing. Therefore, this height is adopted to evaluation standard of heat transfer enhancement, and this value is kept constant throughout the tests here.

5.1 Effect of the Aspact Ration

The first parameter which study its effect on the pinned fin *MCHS* performance is the aspect ratio (*AR*) of the pin, the values of the aspect ratio are (0.138, 0.27, and 0.45) considering the same circumferential area of the pin (0.35×10^{-6} m^2) (exposed to the fluid) and with change perimeter (2.36, 2.78 and 3.71 mm),respectively. The range of this parameter are shown in ***Table (2). Figure .7. (a)– (d)*** show the effect of (*AR*) on the Nusselt number, base temperature, friction factor and *JF* factor for a range of Reynolds numbers at ψ = 1 with respect to the straight baseline plate-fin microchannel. ***Figure .7.*** (a) Show that the Nusselt number increases with increasing the (*AR*) compared with plate-fin heat sink especially at the higher range of Reynolds numbers. The aspect ratio of pins plays an important role in heat transfer enhancement by disturbing the growth of thermal boundary layer. In fact, increase the aspect ratio causes a turbulence in the main flow direction leads to a larger wake region behind the pins and greater heat removal. Increasing the (*AR*) of the pins means decreasing the angle of separation or increasing the wake region and the heat transfer rate or Nusselt number, and vice versa. Moreover, ***Figure 7.(b)*** illustrates the effect of the AR on the substrate base temperature. It can be seen that there is a slight gradient in the base temperature compared to the smooth channel. This gradient in the temperature increases with the increase of the flow rate.

In contrast, the friction factor increases with increasing the *AR* compared with *PFMCHS* as is shown in the ***Figure .7***. (c). At low Reynolds number, some portion of the pins is immersed in the boundary layer without any effect on the thermal performance but only on the hydraulic performance due to the additional pressure drop. It can be seen that the values of friction factors reduce steeply when *Re* number increase. This reduction in friction factor becomes small of the highest values of *Re* number giving an indication that the current result satisfy the moody chart. And this giving an indication that the current result satisfy the search result of ***Wahid et al. [22]***.

Also, the *JF* has a parabolic behavior with the *AR* as shown in ***Figure .7.*** (d).At lowest value of *Re* number, *JF* is reversibly proportional with *AR* and the relationship between them is linear. While, at *Re* = 250 and 500, the two largest aspect ratios show the same enhancement. The highest two values of *Re*, show that the smallest and largest *AR* provide better *JF* enhancement. Where some portion of the pins is embedded in the boundary layer. At highest Reynolds number, *JF* factor decreases and persists until *AR* = 0.27, then it increases. It can be attributed to the fact that at lower values of *Re* number, the hydraulic boundary layer is thick and most of pin height is embedded in the boundary layer. At the case of highest *AR*, the cross-sectional area of the flow is at its smallest values. In contrast, and when *Re* increases, the thickness of boundary layer decreases (i.e., R_{th} decreases) which leads to increase the amount of heat transfer. Besides, the role of the pin for mixing the cold and hot layers of fluid becomes more intensive and consequently increase the turbulence intensity.

The isotherm lines contours and vectors plots of velocity from *CFD* analysis for (*AR* = 0.138, 0.27, 0.45) are depicted in ***Figure .8.*** (a)–(c) respectively. It can be attributed to the fact that at *AR* = 0.138, there is no flow separation behind the pin which is considered as disadvantages, while at *AR* = 0.45, a great recirculation in the flow occurs after the pin making better fluid mixing as it can be seen clearly in ***Figure .8.*** (Left) .It is also observed from the figure that the separation region behind the pin is greater with *AR* = 0.27. The trend is also reflected from the isotherm lines contours ***Figure .8.*** (Right) as the case, *AR* = 0.27 shows the highest temperatures behind the pin. It can be observed from the figure that the best thermal performance is at *AR* = 0.45. This result gives an indication that the best hydrothermal performance can be obtained at large aspect ratio under current conditions, for all cases and for the whole range of Reynolds number, the optimum aspect ratio is *AR* = 0.45 which show highest average Nusselt number ratio is 29.2% at *Re* =1200 compared to the smooth channels, and overall *JF* factor (1.26 times) compared to plate-fin microchannel heat sink.

Table.2. Geometric parameters of pin aspect ratio (*AR*). All dimensions are in (m).

AR	ψ	D_h	d	D	H_P	A_P (m^2)	S
0.138	1	1×10^{-3}	0.25×10^{-3}	1.8×10^{-3}	1.125×10^{-3}	0.35×10^{-6}	5×10^{-3}
0.27	1	1×10^{-3}	0.35×10^{-3}	1.285×10^{-3}	1.125×10^{-3}	0.35×10^{-6}	5×10^{-3}
0.45	1	1×10^{-3}	0.45×10^{-3}	1×10^{-3}	1.125×10^{-3}	0.35×10^{-6}	5×10^{-3}

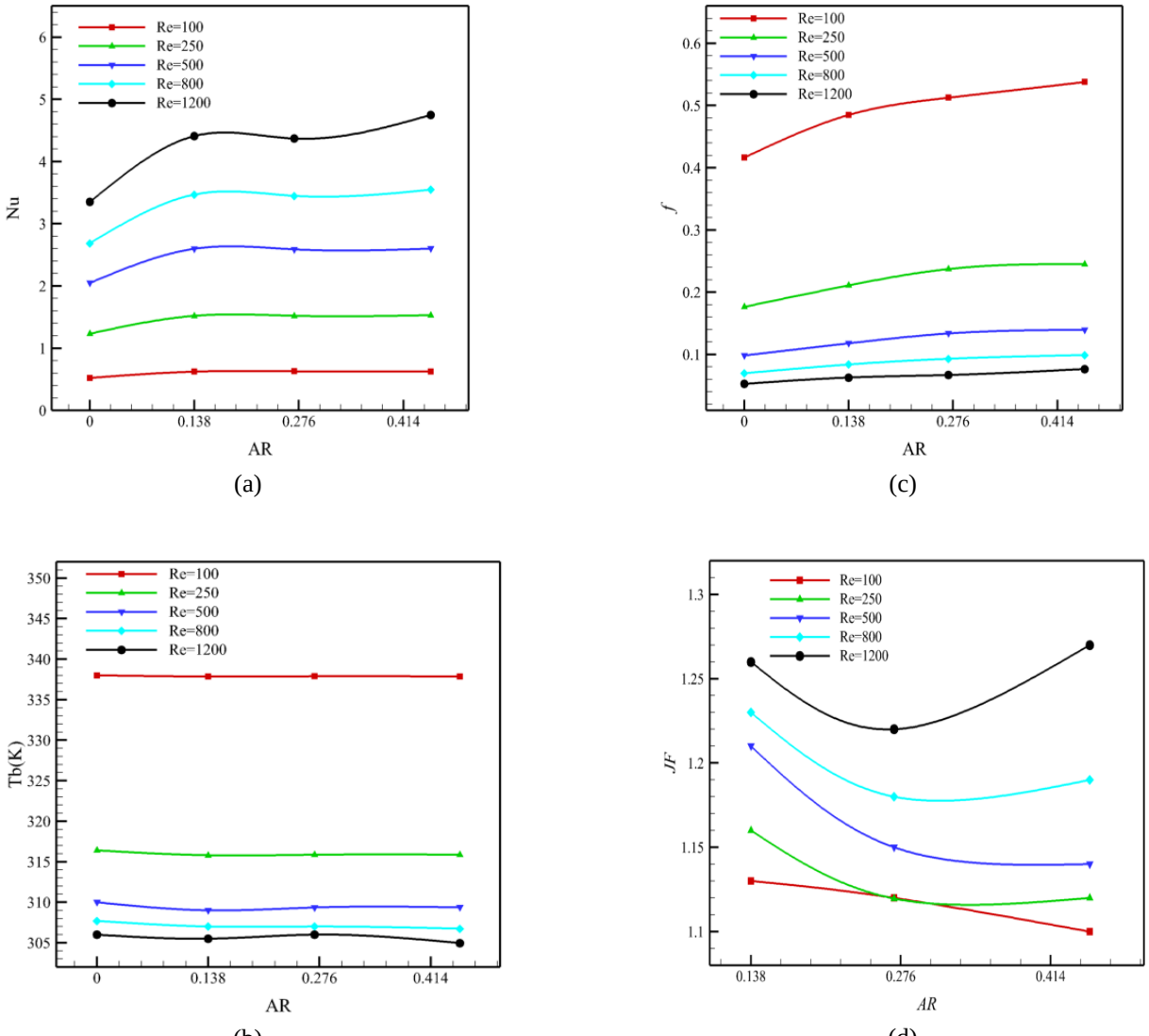

Figure .7. Effect of the aspect ratio (*AR*) on (a) Nusselt number, (b) substrate base temperature, (c) friction factor, and (d) *JF* factor at ψ = 1.

fluid flows. Based on the basic concept of Moody chart, the friction factor reduces with

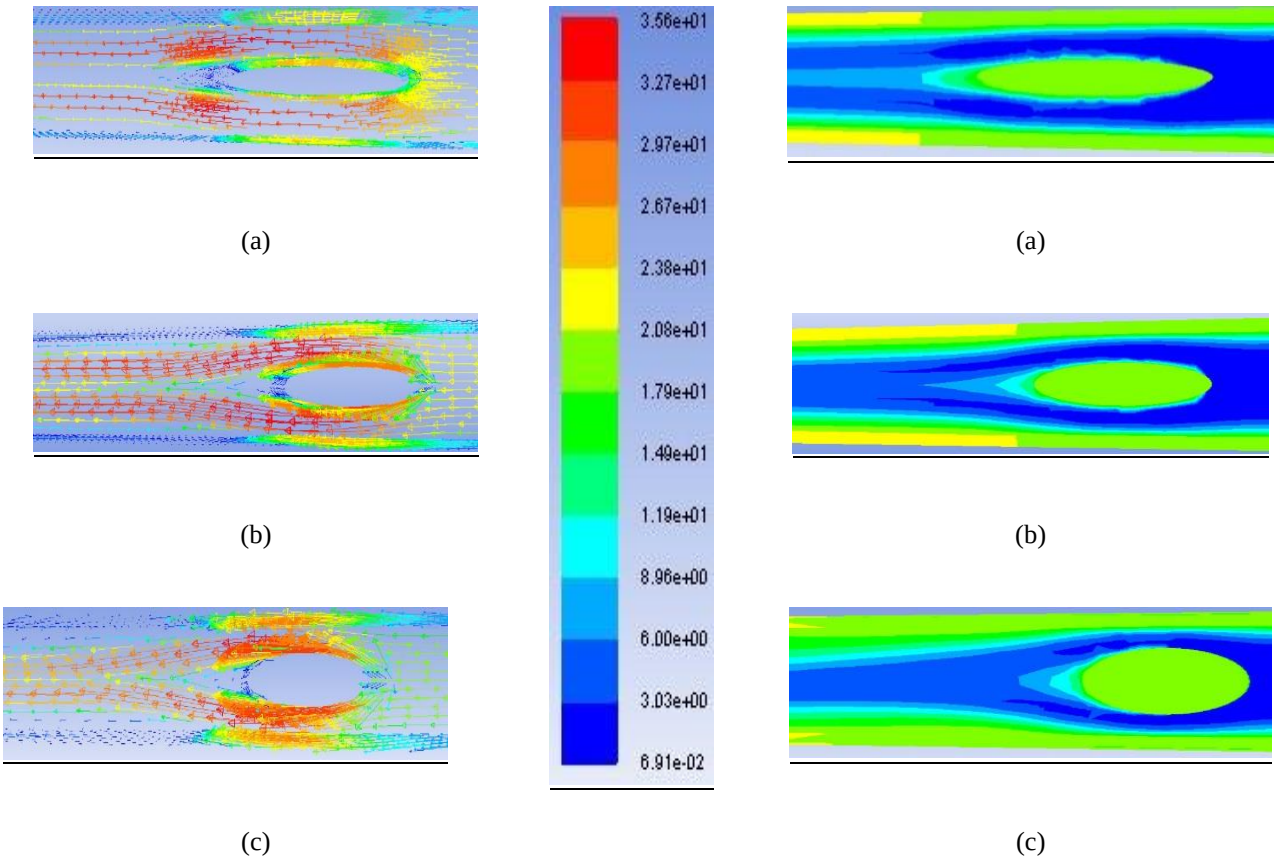

Figure .8. Top view of (Left) Vectors plots of velocity (m/s), and (right) Isotherm lines contours (k) for (a) *AR* = 0.138, (b) *AR* = 0.27, and (c) *AR* = 0.45 at *Re* = 1200 and ψ = 1.

5.2 Effect of the pin number ratio

Figure.9. (a)–(d) show the effect of the pin number ratio $\psi = (N_p/N_c)$ on the Nusselt number, base temperature, friction factor and *JF* factor for the whole range of Reynolds number. The values of pin number ratio considered here are ψ = 0, 1, 2 and 3 respectively, while the other variables are *AR* = 0.27. ***Figure.9. (a)*** Illustrates that the Nusselt number increases with increasing the number of pins. This enhancement is dramatically and monotonically increases with Reynolds number as greatest *Nu* enhancement is (37.52%) which is recorded at *Re* = 1200. ***Figure 9(b)*** exhibits the effect of the pin number on the substrate base temperature. The temperature gradient is clearly observed here with increasing the pin number particularly at the highest rates of the increasing the flow rate. In contrast, an increase in the friction factor is registered with the addition of pins. It can be justified that each pin reduces the cross-sectional area of *the* flow in which the pressure losses increases. It should be remarked that the additional frictional losses decreases with increasing the flow rate as shown in ***Figure 9(c)***. From the figure, it is difficult to judge which case is highest; heat transfer enhancement or frictional losses. This can be answered by going to ***Figure.9.*** (d). It is very clear to say that the hydrothermal behavior *JF* factor noticeably decreases with increasing the pins number at lowest values of Reynolds number and this is giving an indication that the current result satisfy the search result of ***Ahmed [4]***. It persists up to *Re* =

500, while at *Re* = 800 the trend of *JF* is unchanged with ψ and only at the highest value of *Re* the hydrothermal performance (*JF*) factor increases with pin number ratio. It emphasizes that a great *JF* factor with increasing trend can be obtained when *Re* > 800. This is attributed to the fact that a portion of pins is immersed in the hydraulic boundary layer caused an increase in the pressure drop while there is no destroying to the boundary layer. This unexposed portion is reduced with increasing the flow rate (reducing the thickness of boundary layer). Therefore, the best hydrothermal performance for the pin is when *Re* > 800 and a better enhancement can be obtained with increasing N_p, great benefit is observed at higher values of flow rates. ***Figure .10***. (a)–(c), and ***Figure.11***. (a)–(c) show the vectors plots of velocity and isotherm lines contours from *CFD* analysis for the three cases of pin number ratio at *Re* = 1200, *AR* = 0.27. ***Figure .12.*** (a) – (d) show the effect of the pin number ratio (ψ = 0, 1, 2, 3) respectively on the axial Nusselt number for the *Re* = 1200 with respect to the straight baseline plate-fin microchannel. It is worth to be mentioned that the values of pin number ratio considered are *AR* = 0.27.

It is worth to be mentioned the line of *Nu* number is considered at the center line of the base wall of the flow channel passing *through* the out- surface of the pin. It can be seen from ***Figure .***12.that for smooth *MCHS*, *Nu* number starts from its highest value at the beginning of the channel, then reduces with the axial direction toward the exit of the channel till reaches to the fully developed region.When one pin is used after (5×10^{-3}m) from the leading edge of the channel, a great fluctuation in the fluid flow can be seen at and after the location of the pin causing high increase in the local *Nu* number. More deterioration of the heat transfer can be observed when two pins are used. The effect of pins persists continuously with axial direction of the flow toward the channel exit. It shows the effectiveness of using multiple row of pins providing more enhancement for Nusselt number. Moreover, it should be noted that the pitch distance in Figure 12(C) is greater than that in Figure 12(D). Hence, the shortest pitch exhibits uniform local enhancement in the Nusselt number while the longer pitch shows decreasing in the enhancement of the Nusselt number with axial direction. The periodic fluctuation in the flow is obtained by using *three* pins, while the *Nu* = 0.0 at the tip of the pin as it is considered adiabatic in the current boundary conditions.

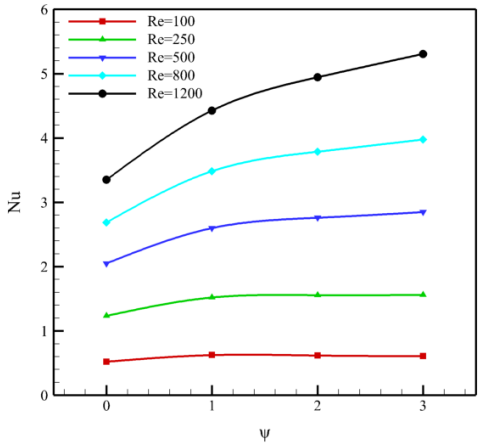

(a)

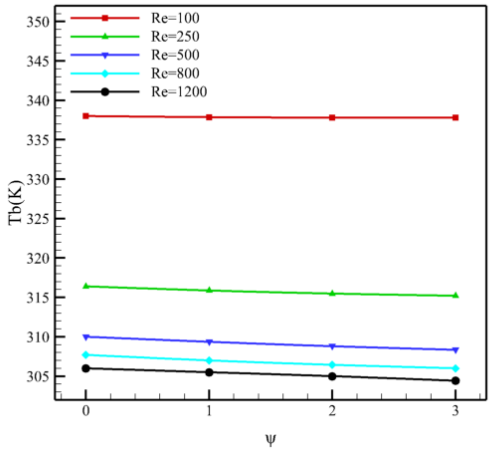

(b)

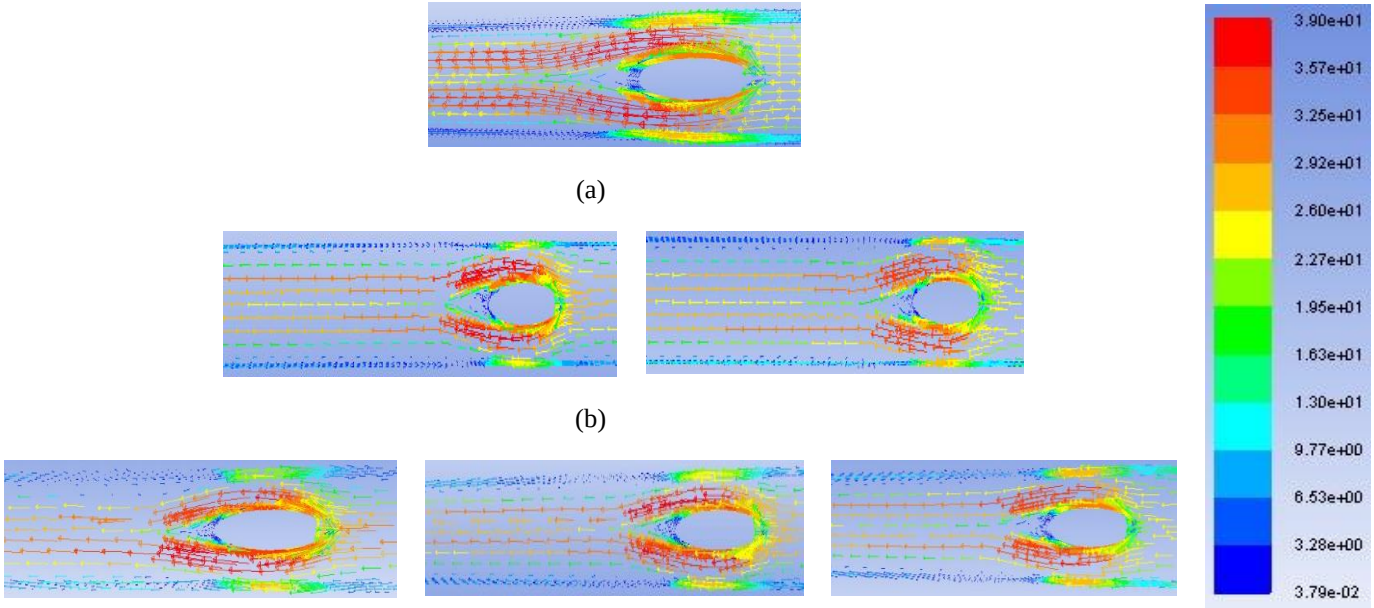

Figure .10. Top view of (up) vectors of Velocity (m/s), for (a) ψ = 1, (b) ψ = 2, and (c) ψ = 3 at *Re* = 1200, *AR* = 0.27.

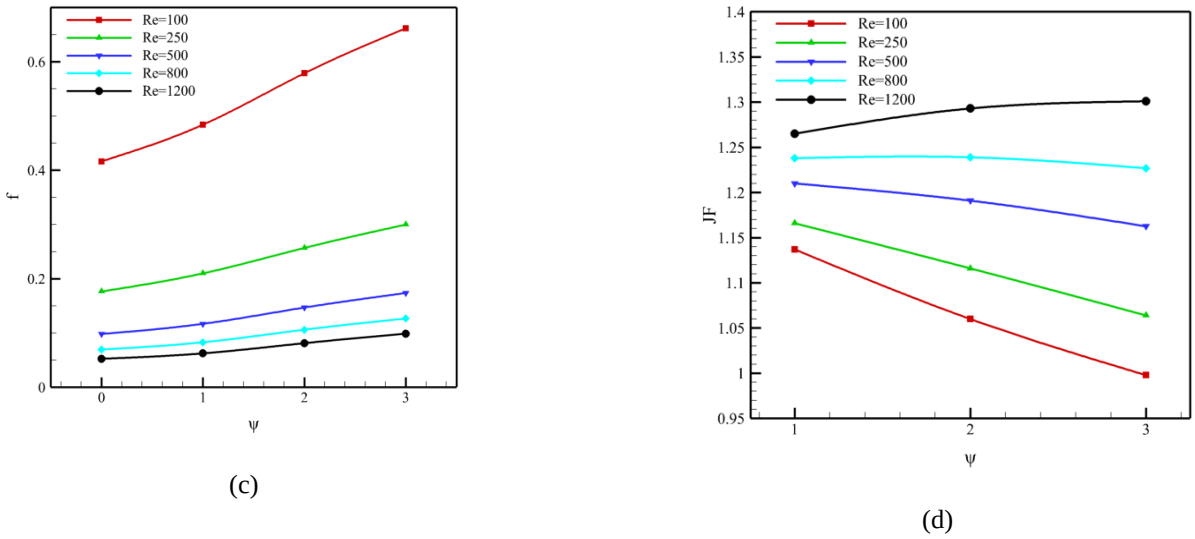

Figure .9. Effect of pin number ratio ψ on (a) Nusselt number, (b) substrate base temperature, (c) friction factor, and (d) *JF* factor at *AR* =0.27.

5.3 Overall Hydrothermal Performance

To show the overall performance of the two parameters; *AR*, ψ, the overall *JF* factor for all *Re* numbers is estimated and depicted as illustrated in ***Figure.13.*** (a) - (b) respectively. ***Figure.13.*** (a) shows that the best hydrothermal performance is obtained at the smallest aspect ratio which is around overall *JF* = 1.2. In addition, the trend of overall *JF* is going down with the pin number ratio, starting from 1.2 to 1.15 as observed in the subfigure (b).

5.4 Mechanical Fan Power Reduction

In the last part of the current study is to examine the effect of using single pin in each channel with ψ = 1 and D_h =1 ×10^{-3} m, on the pressure drop and mechanical fan power reduction. For the case of plate-fin channel, Nusselt number is (3.35) at *Re* = 1200. By using pin, the Nusselt number ratio is greatly enhanced. To get the same value of Nusselt number of smooth channel (i.e., Nu^*/ Nu_o = 1), the flow rate must be reduced when the pin is used. By this way, Reynolds number is reduced up to 770 for the pinned fin *MCHS* to provide same thermal performance of smooth one as shown in Figure 14.

It could be deduced that the mechanical fan power required for pushing the fluid in *PFMCHS* decreases in the case of pinned fin *MCHS* for the corresponding amount of the heat transfer rate. In that case, a reduction in the mechanical fan power is obtained around (57%) and this gives an indication that the current result satisfy the search result of ***Ahmed [4]*** as shown in Table 3.

Table 3. Mechanical fan power reduction by using pin.

variables	No pin	pinned
Nu	3.35	3.35
Re	1200	770
u (m/s)	21.8	14.1
ΔP (Pa)	764.4	505
mechanical fan power (W)	0.15185	0.064886
Power reduction (%)	-	57

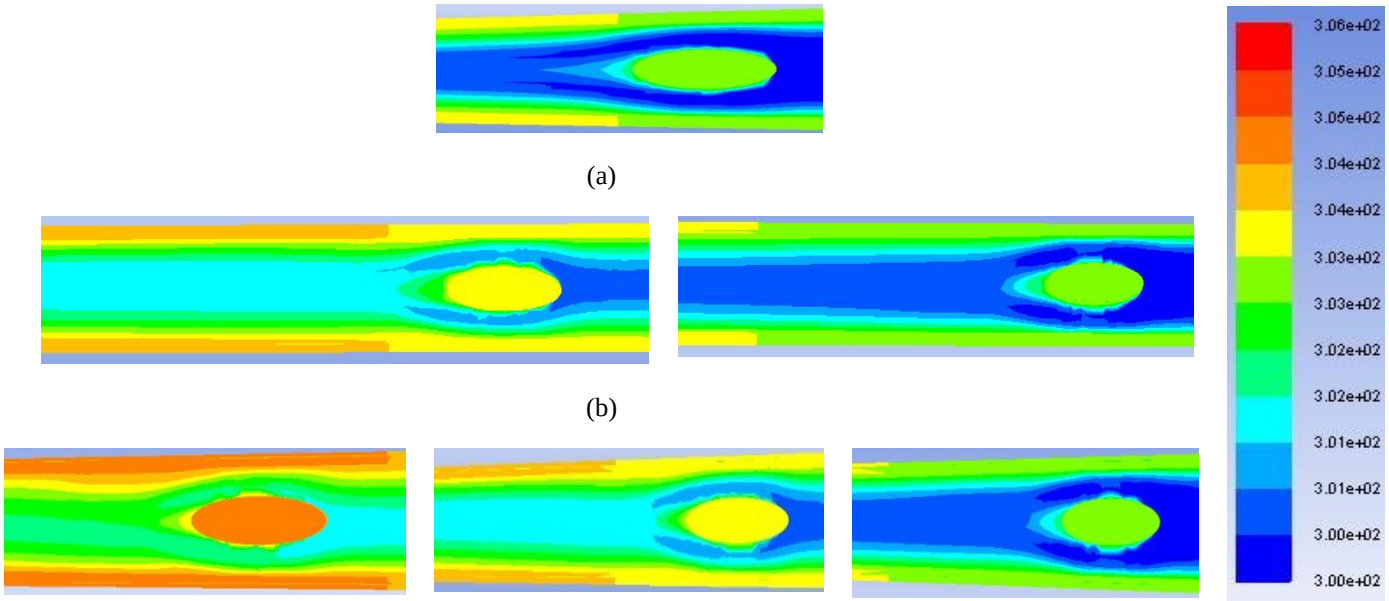

(a)

(b)

(c)

Figure .11. Top view of Isotherm lines contours (*K*) for (a) ψ = 1, (b) ψ = 2, and (c) ψ = 3 at *Re* = 1200, *AR* = 0.27.

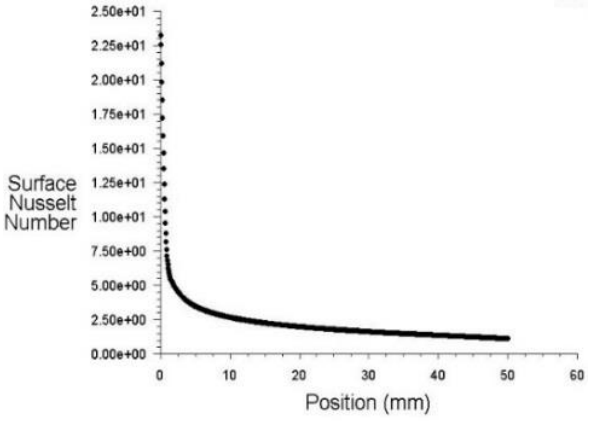

(a)

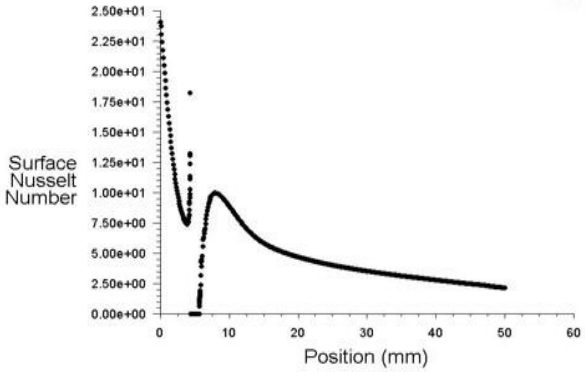

(b)

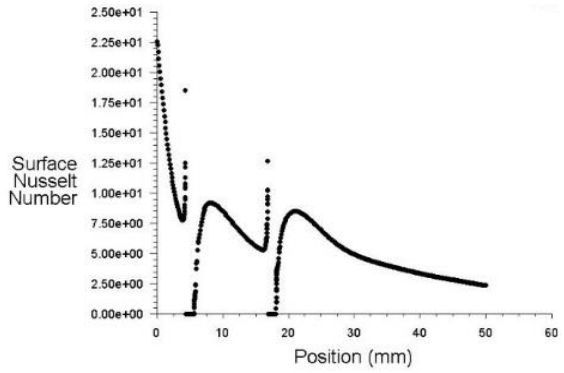

(c)

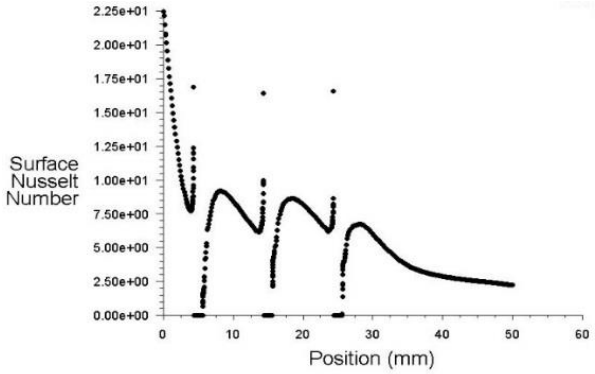

(d)

Figure .12. Effect of pin number ratio ψ on surface Nusselt number for (a) ψ = 0, (b) ψ = 1, (c) ψ = 2, and (d) ψ = 3 at *Re* = 1200, *AR* =0.27.

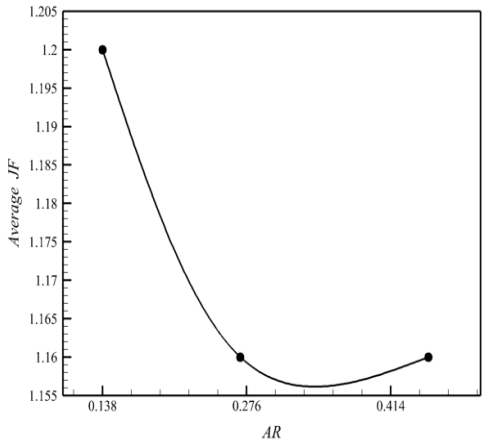

(a)

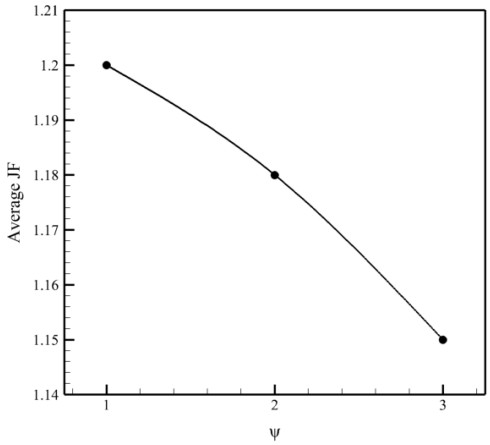

(b)

Figure .13. Overall hydrothermal performance of (a) *AR* and (b) pin number ψ.

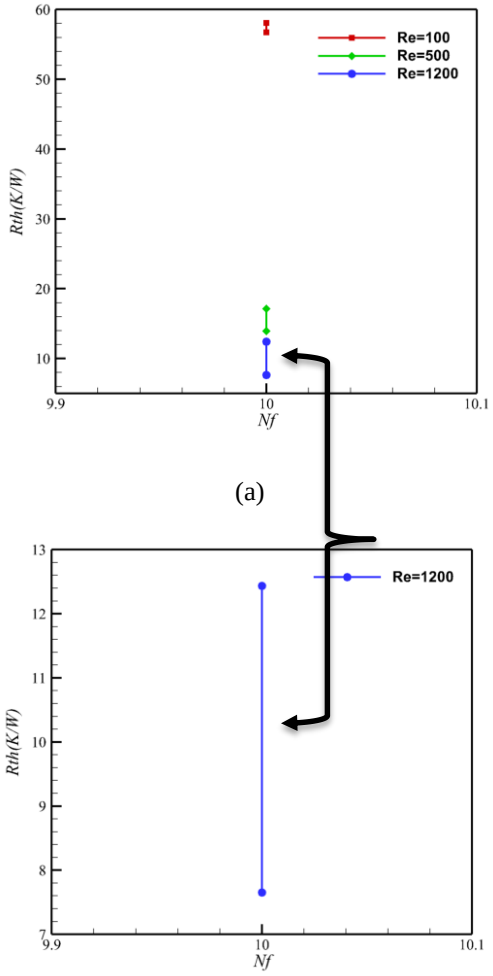

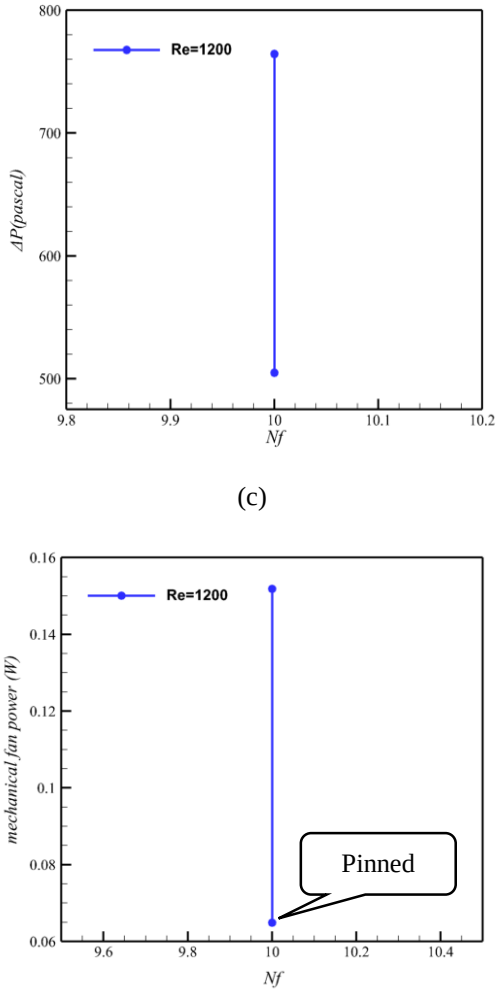

Figure .14. Effect of using single pin on (a) R_{th} at *Re* = 100, 500, 1200, (b) *Re* = 1200, (c) pressure drop at *Re* = 1200, and (d) mechanical fan power at *Re* = 1200.

6. Conclusion

The main aim of this numerical work is to optimize the hydrothermal performance of pinned fin *MCHS* by considering uninvestigated design of pins installed in the microchannels. Different aspect ratios, numbers of pins are the variable parameters in this investigation. The *CFD* results can be concluded briefly as follows:

1- The best hydrothermal performance is observed at the pins aspect ratio of (*AR* = 0.45) which shows best overall Nusselt number ratio (1.3 times) and *JF* factor (1.20) compared to plate-fin microchannel heat sink.

In contrary, this performance is observed to reduce at higher than this value of *AR*.

2-The *MCHS* with pins provides better hydrothermal performance than smooth one at pin number ratio of (ψ = 1) as the best overall Nusselt number ratio is around (1.26 times) and *JF* factor (1.20) compared to plate-fin *MCHS*. It is decreased when this ratio increases.

3-Maximum mechanical fan power reduction obtained is about 57% for the pinned fin *MCHS* with ψ= 1 and D_h =1 ×10^{-3} m compared to the corresponding original channel heat sink.
4- It is seen that the thermal resistance of the pinned fin *MCHS* is about 50% lower, and the pressure drop of the pinned fin *MCHS* is much higher than that of the plate-fin *MCHS* under the same conditions. As the pressure drop is directly proportional to the mechanical fan power required to move the cooling air through the heat sink, and shows that the *JF* factor decreases as the mechanical fan power increases, and the *JF* factor of the pinned fin MCHS is about 24% higher than that of the original one under same mechanical fan power. This indicates that the pinned fin MCHS needs less mechanical fan power than the original one when the heat dissipation power is the same for the two types of heat sinks. Therefore, adopting the pinned fin *MCHS* can make the volume of air-cooling system smaller.

7. Recommendation For Future Works

This investigation leaves a wide scope of recommendations and suggestions for future studies as an extension of the current work.

1. Study the effect of perforated oval pins on the hydrothermal design of plate-fin heat sink.
2. Change the perforation in the previous point to Slots.
3. Oval pins having notches can be examined numerically too.
4. Replace the air coolant by nanofluids for further heat absorption by the coolant but it associates a higher pressure drop as well.

Nomenclature:

A	area m^2
A_h	convection heat transfer area m^2
D_h	hydraulic diameter m
f	friction factor
h_z	local convection heat transfer coefficient W/m^2 K
H	Height m
c_p	Specific heat J/kg K
JF	performance evaluation criterion
k	thermal conductivity W/m K
L	Length m
N	Number of fins
Nu	Nusselt number
P	Pressure Pa
Δ_P	Pressure drop Pa
x, y, z	Cartesian coordinates in X, Y, and Z direction
d	small diameter of elliptical pin m
D	large diameter of elliptical pin m
AR	Aspect ratio
ΔT	temperature difference K

Greek symbols

ψ	pin number ratio
ρ	Density kg/m^3
α	thermal diffusivity m^2/ s^2
μ	dynamic viscosity kg/m .s
ϑ	Kinematic viscosity m^2/s

Subscripts

$*$	modified case
avg	Average
R_{th}	thermal resistance K/W
$M.\ F.P$	mechanical fan power W
q	heat flux W/m^2
Q	heat transfer W

$\dot{V}$	mass flow rate m^3/s
P_P	pins pitch m
Re	Reynolds number
S	pitch distance between the beginning of the channel and the first pin center m
W	Width m
T	Temperature K
u, v, w	velocity components in x, y and z directions, respectively m/s
U, V, W	dimensionless velocity components in x, y, z direction, respectively

b	base of substrate
c	Channel
f	Fin
f	fluid zone
in	inlet
m	mean
o	original case
p	Pin
w	wall
out	Outlet

Abbreviation

PFMCHS	plate-fin microchannel heat sink

References

[1] Seri Lee, "Optimum Design and Selection of Heat Sinks," Eleventh IEEE SEMI-THERM Symposium, (1995) pp. 48-54.

[2] Xiaoling Yu, Jianmei Feng, Quanke Feng, Qiuwang Wang, Development of a plate-pin fin heat sink and its performance comparisons with a plate fin heat sink, Applied Thermal Engineering 25(2005) pp. 173–182.

[3] Guilian Wang, Di Niu, Fuqiang Xie, Yan Wang, Xiaolin Zhao, Guifu Ding, Experimental and numerical investigation of a microchannel heat sink (MCHS) with micro-scale ribs and grooves for chip cooling, Applied Thermal Engineering 85(2015) pp. 61-70.

[4] Hamdi E. Ahmed, Optimization of thermal design of ribbed flat-plate fin heat sink, Applied Thermal Engineering 102 (2016)pp. 1422–1432.

[5] Hans Jonsson and Bahram Moshfegh, Modeling of the Thermal and Hydraulic Performance of Plate Fin, Strip Fin, and Pin Fin HeatSinks-Influence of Flow Bypass, Ieee Transactions On Components And Packaging Technologies, No. 2, June 2001, Vol. 24.

[6] Fangjun Hong and Ping Cheng, Three dimensional numerical analyses and optimization of offset strip-fin microchannel heat sinks, International Communications in Heat and Mass Transfer 36(2009) pp. 651–656.

[7] Chao Liu, Jyh-tong Teng, Jian-Cherng Chu, Yi-lang Chiu, Suyi Huang, Shiping Jin, Thanhtrung Dang, Ralph Greif, Hsin-Hung Pan f, Experimental investigations on liquid flow and heat transfer in rectangular microchannel with longitudinal vortex generators, International Journal of Heat and Mass Transfer 54(2011) pp. 3069–3080.

[8] Beom Seok Kim, Bong Seop Kwak, Sangwoo Shin, Sanghoon Lee, Kyung Min Kim, Hyo-Il Jung, Hyung Hee Cho, Optimization of microscale vortex generators in a microchannel using advanced response surface method, International Journal of Heat and Mass Transfer 54(2011) pp. 118–125.

[9] Hung-Yi Li, Ci-Lei Chen, Shung-Ming Chao, Gu-Fan Liang, Enhancing heat transfer in a plate-fin heat sink using delta winglet vortex generators, International Journal of Heat and Mass Transfer 67(2013) pp. 666-677.

[10] Amin Ebrahimi, Ehsan Roohi, Saeid Kheradmand, Numerical study of liquid flow and heat transfer in rectangular microchannel with longitudinal vortex generators, Applied Thermal Engineering 78(2015) pp. 576-583.

[11] Li Zhuo, Tao Wen-Quan, He Ya-Ling, A numerical study of laminar convective heat transfer in microchannel with non-circular cross-section, International Journal of Thermal Sciences 45(2006) pp. 1140–1148.

[12] Guodong Xia, Lei Chai, Haiyan Wang, Mingzheng Zhou, Zhenzhen Cui, Optimum thermal design of microchannel heat sink with triangular reentrant cavities, Applied Thermal Engineering 31(2011) pp.1208-1219.

[13] Lei Chai, Guodong Xia, Mingzheng Zhou, Jian Li, Numerical simulation of fluid flow and heat transfer in a microchannel heat sink with offset fan-shaped reentrant cavities in sidewall, International Communications in Heat and Mass Transfer 38(2011) pp. 577–584.

[14] Chi-Chuan Wang, Kai-Shing Yang, Yang-Ping Liu, Ing Youn Chen, Effect of cannelure fin configuration on compact air cooling heat sink, Applied Thermal Engineering 31(2011) pp. 1640-1647.

[15] Hamdi E. Ahmed, Mirghani I. Ahmed, Optimum thermal design of triangular, trapezoidal and rectangular grooved microchannel heat sinks, International Communications in Heat and Mass Transfer 66(2015) pp. 47-57.

[16] H.A. Mohammed, P. Gunnasegaran, and N.H. Shuaib, Numerical simulation of heat transfer enhancement in wavy microchannel heat sink, International Communications in Heat and Mass Transfer 38(2011) pp. 63–68.

[17] H.A. Mohammed, P. Gunnasegaran, N.H. Shuaib, Influence of channel shape on the thermal and hydraulic performance of microchannel heat sink, International Communications in Heat and Mass Transfer 38(2011) pp. 474–480.

[18] Muhammad Mustafizur Rahman, Measurement of heat transfer in microchannel heat sinks, Heat Mass Transfer, Vol. 27, No. 4, (2000) pp. 495-506.

[19] Mohamed R. Shaalan, Mohamed A. Saleh, Osama Mesalhy, Mohamed L. Elsayed, Thermo/fluid performance of a shielded heat sink, International Journal of Thermal Sciences 60 (2012)pp. 171-181.

[20] Hung-Yi Li, Go-Long Tsai, Shung-Ming Chao, Yi-Feng Yen, Measurement of thermal and hydraulic performance of a plate-fin heat sink with a shield, Experimental Thermal and Fluid Science 42(2012) pp. 71-78.

[21] Hamdi E. Ahmed, B.H. Salman, A.Sh. Kherbeet, M.I. Ahmed, Optimization of thermal design of heat sinks: A review, International Journal of Heat and Mass Transfer 118(2018) pp.129–153.

[22] Mazlan A. Wahid, Ahmad Ali Gholami, H.A. Mohammed, Numerical Study of Fluid Flow and Heat Transfer Enhancement of Nanofluids over Tube Bank, Applied Mechanics and Materials Vol. 388(2013) pp.149-155.

[23] Gawande, V.B., Dhoble, A.S., Zodpe, D.B., 2014b. CFD analysis to study effect of circular vortex generator placed in inlet section to investigate heat transfer aspects of solar air heater. Sci. World J. http://dx.doi.org/10.1155/(2014)/567257.

[24] Kumar, A, Bhagoria, J.L., Sarviya, R.M., 2008. In: International 19th National & 8th ISHMT-ASME Heat and Mass Transfer Conference Heat Transfer Enhancement in Channel of Solar Air Collector by using Discrete w-shaped Artificial Roughened Absorber.

[25] M.R. Sohel , S.S. Khaleduzzaman , R. Saidur , A. Hepbasli , M.F.M. Sabri , I.M. Mahbubul, An experimental investigation of heat transfer enhancement of a minichannel heat sink using $Al_2O3–H_2O$ nanofluid , International Journal of Heat and Mass Transfer 74(2014) pp. 164–172.